Novel lanthanide(III)/gallium(III) metallacrowns with appended visible-absorbing organic sensitizers for molecular near-infrared imaging of living cells†

Timothée Lathion,[a] Julie Bourseguin,[b] Svetlana V. Eliseeva,*[b] Matthias Zeller,[c] Stéphane Petoud*[b] and Vincent L. Pecoraro*[a]

[a.] *Department of Chemistry, Willard H. Dow Laboratories, University of Michigan, Ann Arbor, Michigan 48109-1055, USA. E-mail: vlpec@umich.edu*
[b.] *Centre de Biophysique Moléculaire, CNRS UPR 4301, Université d'Orléans, Orléans 45071, France. E-mail: svetlana.eliseeva@cnrs-orleans.fr; stephane.petoud@inserm.fr*
[c.] *Department of Chemistry, Purdue University, 560 Oval Drive, West Lafayette, Indiana 47907, USA*

Table of contents

1. Organic synthesis

Reagents and chemicals. All reagents and chemicals were purchased from commercial sources and used without further purification unless otherwise stated. Silica (215–400 mesh) was used for flash column chromatography. 5-Maleimido-isophthalic acid **H_2mip**,[1] 7-(diethylamino)-3-coumarin carboxylic acid **3**[2–5] and *S*-tritylcysteamine linker **6**[6] were synthesized according to or by modifying existing procedures (Scheme S1). ^{1}H and ^{13}C NMR spectra of synthesized molecules are presented in Figures S1-S8.

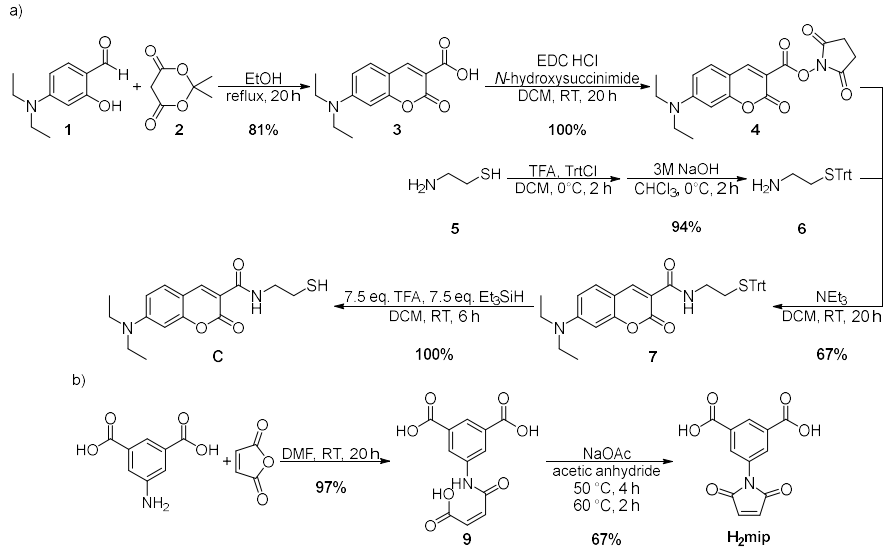

Scheme S1. a) Synthesis of the thiol-coumarin antenna **C**. b) Synthesis of the **H_2mip** bridging ligand.[1]

Synthesis of *S*-tritylcysteamine (6). 3.75 g of cysteamine hydrochloride (**5**, 33.0 mmol, 1.1 eq.) were placed under N_2 to which 17 mL of CH_2Cl_2 were added. The resulting solution was cooled down to 0 °C. 7 mL of trifluoroacetic acid were added dropwise to the solution, followed by 8.36 g of trityl chloride (30.0 mmol, 1.0 eq.). The solution was then maintained at 0 °C for 2 h. The solution was evaporated to dryness and suspended in 30 mL of $CHCl_3$. 10 mL of NaOH 10 M were added, and the solution was vigorously stirred for 1 h at room temperature. The organic phase was collected and the aqueous phase extracted with $CHCl_3$ (3x 40 mL). The organic phases were reunited, washed with half-saturated aq. NaCl (2x 50 mL), dried over anhydrous $MgSO_4$, filtered and evaporated to dryness to give 9.02 g of *S*-tritylcysteamine as a yellowish solid (**6**, 28.2 mmol, 94%). ^{1}H NMR (CD_2Cl_2, 500 MHz) δ, ppm: 7.43 (6H, d, ^3J = 7.5 Hz), 7.29 (6H, t, ^3J = 7.7 Hz), 7.22 (3H, t, ^3J = 7.2 Hz), 2.55 (2H, t, ^3J = 6.8 Hz), 2.27 (2H, t, ^3J = 6.5 Hz), 1.17 (2H, s).

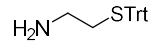

6

Synthesis of 7-(diethylamino)-coumarin-3-carboxylic acid (3). 4.28 g of 4-(diethylamino)-salicylaldehyde (1, 22.1 mmol, 1.0 eq.) and 3.83 g of Meldrum's acid (**2**, 2,2-dimethyl-1,3-dioxane-4,6-dione, 26.6 mmol, 1.2 eq.) were dissolved in 25 mL of ethanol. The solution was refluxed overnight then cooled down to room temperature and filtered using a Büchner funnel. The brown solid was washed with cold ethanol to give a bright orange solid that was further recrystallized from boiling ethanol to afford 4.65 g of 7-(diethylamino)-coumarin-3-carboxylic acid as bright red needles (**3**, 17.8 mmol, 81%). ^{1}H NMR ($CDCl_3$, 500 MHz) δ, ppm: 12.34 (1H, bs), 8.64 (1H, s), 7.45 (1H, d, ^3J = 9.0 Hz), 6.70 (1H, dd, ^3J = 9.0 Hz, ^4J = 2.5 Hz), 6.52 (1H, d, ^4J = 2.5 Hz), 3.49 (4H, q, ^3J = 7.1 Hz), 1.26 (6H, t, ^3J = 7.0 Hz).

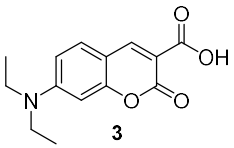
3

Synthesis of 7-(diethylamino)-coumarin-3-carboxylic-*N*-succinimide ester (4). 1.14 g of 7-(diethylamino)-coumarin-3-carboxylic acid (**3**, 4.36 mmol, 1.0 eq.) were placed under N_2 and dissolved in 55 mL of dry CH_2Cl_2. 753 mg of *N*-hydroxysuccinimide (6.54 mmol, 1.5 eq.) and 1.00 g of EDC hydrochloride (5.22 mmol, 1.2 eq.) were added and the solution was stirred overnight at room temperature. The solution was diluted to 150 mL with CH_2Cl_2 and the organic phase was washed with half-saturated aq. $NaHCO_3$ (2x 80 mL) and half-saturated aq. NH_4Cl (2x 80 mL). The organic phase was dried over anhydrous $MgSO_4$, filtered, and evaporated to dryness to give 1.56 g of 7-(diethylamino)-coumarin-3-carboxylic-*N*-succinimide ester as a bright yellow solid (**4**, 4.35 mmol, 100%). ^{1}H NMR ($CDCl_3$, 500 MHz) δ, ppm: 8.58 (1H, s), 7.38 (1H, d, ^3J = 9.0 Hz), 6.64 (1H, dd, ^3J = 9.0 Hz, ^4J = 2.5 Hz), 6.47 (1H, d, ^4J = 2.5 Hz), 3.48 (4H, q, ^3J = 7.1 Hz), 2.88 (4H, s), 1.26 (6H, t, ^3J = 7.0 Hz). ESI-MS (soft positive mode, m/z): [**4**+H]$^+$: 359.12 (exp.), 359.12 (calc.); [**4**+Na]$^+$: 381.11 (exp.), 381.11 (calc.).

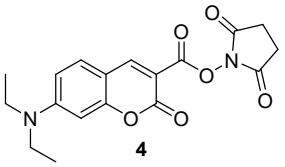
4

Synthesis of 7-(diethylamino)-coumarin-*N*-(2-(tritylthio)ethyl)-3-carboxamide (7). Under N_2, 840 mg of 7-(diethylamino)-coumarin-3-carboxylic-*N*-succinimide ester (**4**, 2.34 mmol, 1.0 eq.) in 20 mL of dry CH_2Cl_2 were added dropwise to 20 mL of a dry CH_2Cl_2 solution containing 974 mg of *S*-tritylcysteamine (**6**, 3.05 mmol, 1.3 eq.) and 425 µL of triethylamine (3.05 mmol, 1.3 eq.). The stirring was maintained overnight at room temperature. The solution was diluted to 80 mL with CH_2Cl_2 and poured in 50 mL of aq. HCl 5%. The organic fraction was collected and the aqueous phase was extracted with CH_2Cl_2 (3x 30 mL). The organic phases were reunited, washed with half-saturated aq. $NaHCO_3$ (2x 50 mL), half-saturated aq. NH_4Cl (2x 50 mL), dried over anhydrous $MgSO_4$, filtered and evaporated to dryness. The yellow solid was further purified by flash column chromatography (SiO_2, CH_2Cl_2/MeOH 100:1.5) to yield 880 mg of 7-(diethylamino)-coumarin-

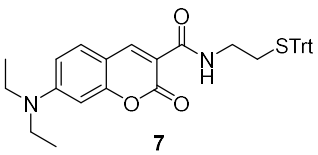
7

N-(2-(tritylthio)ethyl)-3-carboxamide as a yellow solid (**7**, 1.56 mmol, 67%). ^{1}H NMR (CD_2Cl_2, 500 MHz) *δ*, ppm: 8.76 (1H, t, ^{3}J = 5.7 Hz), 8.61 (1H, s), 7.45-7.42 (7H, m), 7.31-7.27 (6H, m), 7.24-7.20 (3H, m), 6.67 (1H, dd, ^{3}J = 9.0 Hz, ^{4}J = 2.5 Hz), 6.51 (1H, d, ^{4}J = 2.5 Hz), 3.46 (4H, q, ^{3}J = 7.2 Hz), 3.27 (2H, q, ^{3}J = 6.4 Hz), 2.43 (2H, t, ^{3}J = 7.0 Hz), 1.23 (6H, t, ^{3}J = 7.0 Hz). HR-ESI-MS (soft positive mode, m/z): [**7**+H]$^{+}$: 563.2349 (exp.), 563.2368 (calc.).

Synthesis of 7-(diethylamino)-coumarin-*N*-(2-mercaptoethyl)-3-carboxamide (C). 300 mg of 7-(diethylamino)-coumarin-*N*-(2-(tritylthio)ethyl)-3-carboxamide (**7**, $5.33 \cdot 10^{-1}$ mmol, 1.0 eq.) were placed under N_2 and dissolved in 4.5 mL of CH_2Cl_2. 305 µL of trifluoroacetic acid (3.99 mmol, 7.5 eq.) and 640 µL of triethylsilane (3.99 mmol, 7.5 eq.) were added and the solution was kept at room temperature for 3 h. The solution was then evaporated to dryness and the solid triturated with petroleum ether (6x 15 mL) to yield 170 mg of 7-(diethylamino)-coumarin-*N*-(2-mercaptoethyl)-3-carboxamide as a bright yellow solid (**C**, $5.31 \cdot 10^{-1}$ mmol, 100%). ^{1}H NMR ($CDCl_3$, 500 Mhz) *δ*, ppm: 9.38 (1H, t, ^{3}J = 6.3 Hz), 8.72 (1H, s), 7.45 (1H, d, ^{3}J = 9.0 Hz), 6.67 (1H, dd, ^{3}J = 9.0 Hz, ^{4}J = 2.5 Hz), 6.50 (1H, d, ^{4}J = 2.5 Hz), 3.65 (2H, q, ^{3}J = 6.4 Hz), 3.47 (4H, q, ^{3}J = 7.2 Hz), 2.76 (2H, dt, ^{3}J = 8.8, 6.8 Hz), 1.48 (1H, t, ^{3}J = 8.5 Hz), 1.25 (6H, t, ^{3}J = 7.0 Hz). ^{13}C ($CDCl_3$, 125 MHz), *δ*, ppm: 164.55, 162.88, 157.93, 153.11, 148.93, 131.67, 110.45, 108.94, 108.57, 96.76, 45.36, 43.24, 24.42, 12.55. HR-HR-ESI-MS (soft positive mode, m/z): [**C**+H]$^{+}$: 321.1265 (exp.), 321.1273 (calc.).

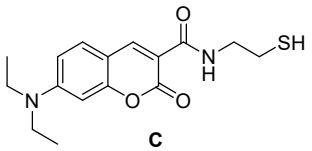

C

Synthesis of 5-(3-carboxyacrylamido) isophthalic acid (9). 5.0 g of 5-aminoisophthalic acid hydrate (25.1 mmol, 1.0 eq.) and 2.71 g of maleic anhydride (27.6 mmol, 1.1 eq.) were dissolved in 35 mL of dimethylformamide. The solution was stirred at room temperature for 6 h and then evaporated to dryness. The solid was dispersed in 250 mL of acetone, filtered using a Büchner funnel and washed with 100 mL of acetone to yield 6.51 g of 5-(3-carboxyacrylamido) isophthalic acid as an off-white solid (**9**, 23.3 mmol, 93%). ^{1}H NMR (DMSO-d_6, 500 MHz) *δ*, ppm: 13.18 (3H, bs), 10.66 (1H, s), 8.46 (2H, s), 8.18 (1H, s), 6.48 (1H, d, ^{3}J = 12.0 Hz), 6.33 (1H, d, ^{3}J = 12.0 Hz).

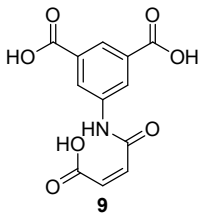

9

Synthesis of H_2mip. 2.72 g of 5-(3-carboxyacrylamido) isophthalic acid (9, 9.74 mmol, 1.0 eq.) were suspended in 19 mL of acetic anhydride and 660 mg of sodium acetate trihydrate (4.87 mmol, 0.5 eq.) were added. The solution was stirred at 50 °C for 4 h, at 60 °C for 2 h and then evaporated to dryness at 40°C. The solid was allowed to cool down to room temperature and resuspended in 300 mL of water under vigorous stirring for 20 min. The solid was filtered using a Büchner funnel and washed with 150 mL of water to afford 1.7 g of the **H_2mip** bridging ligand as a white solid (6.51 mmol, 67%). ^{1}H NMR (DMSO-d_6, 500 MHz) *δ*, ppm: 13.49 (2H, bs), 8.45 (1H, t, ^{4}J = 1.7 Hz), 8.18 (2H, d, ^{4}J = 1.5 Hz), 7.23 (2H, s). HR-ESI-MS (soft negative mode, m/z): [**H_2mip**-H]$^{-}$: 260.0195 (exp.), 260.0195 (calc.).

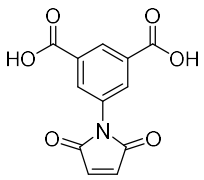

H_2mip

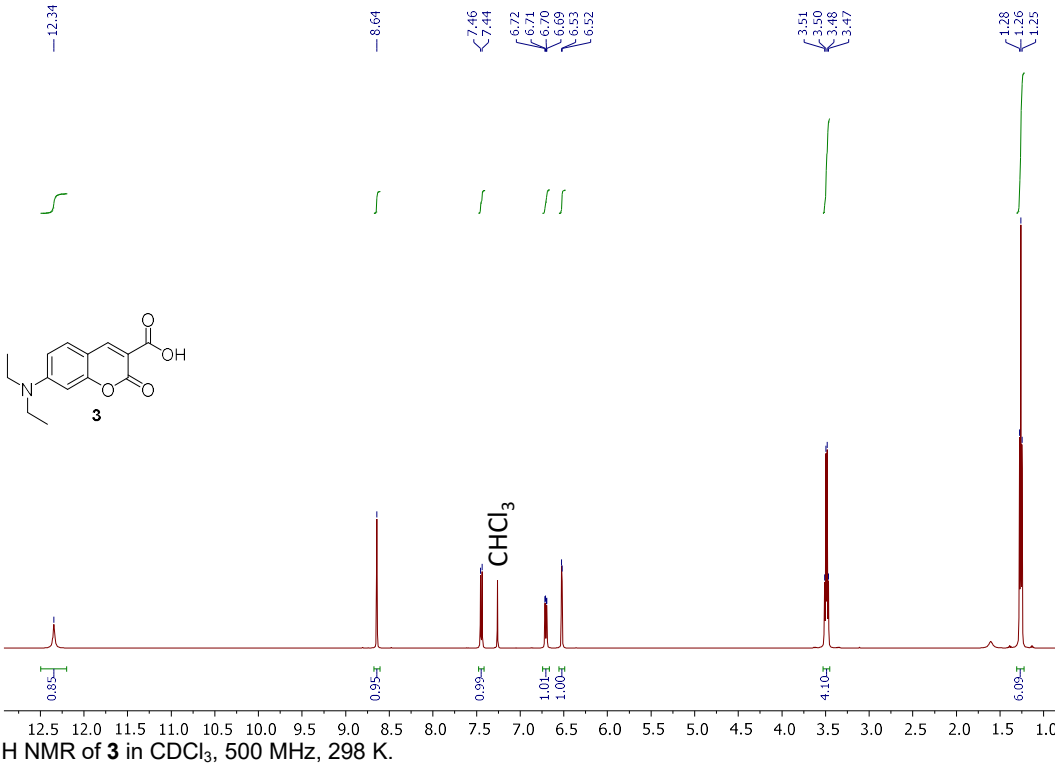

Figure S1. ^{1}H NMR of **3** in $CDCl_3$, 500 MHz, 298 K.

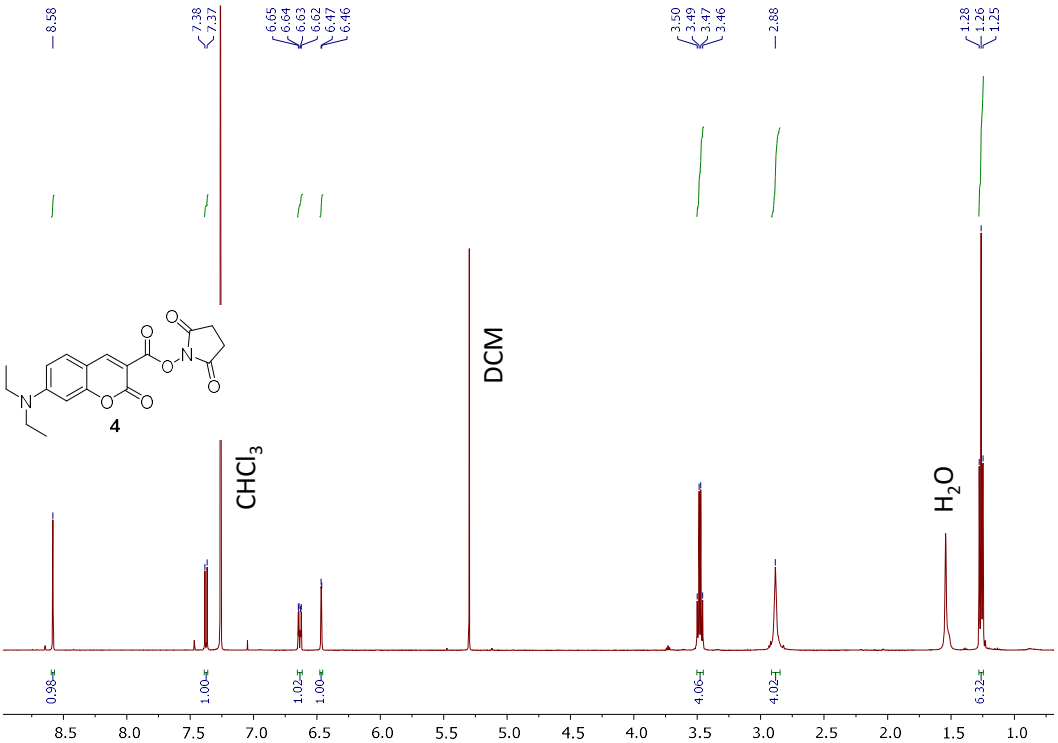

Figure S2. ^{1}H NMR of **4** in $CDCl_3$, 500 MHz, 298 K.

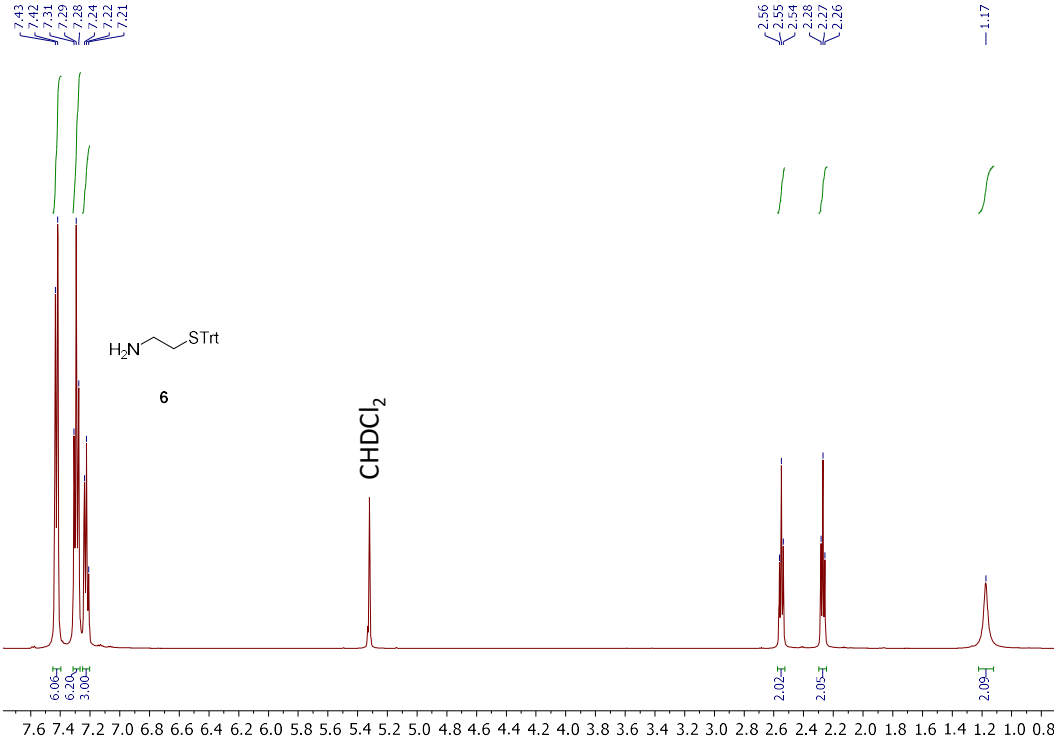

Figure S3. ^{1}H NMR of **6** in CD_2Cl_2, 500 MHz, 298 K.

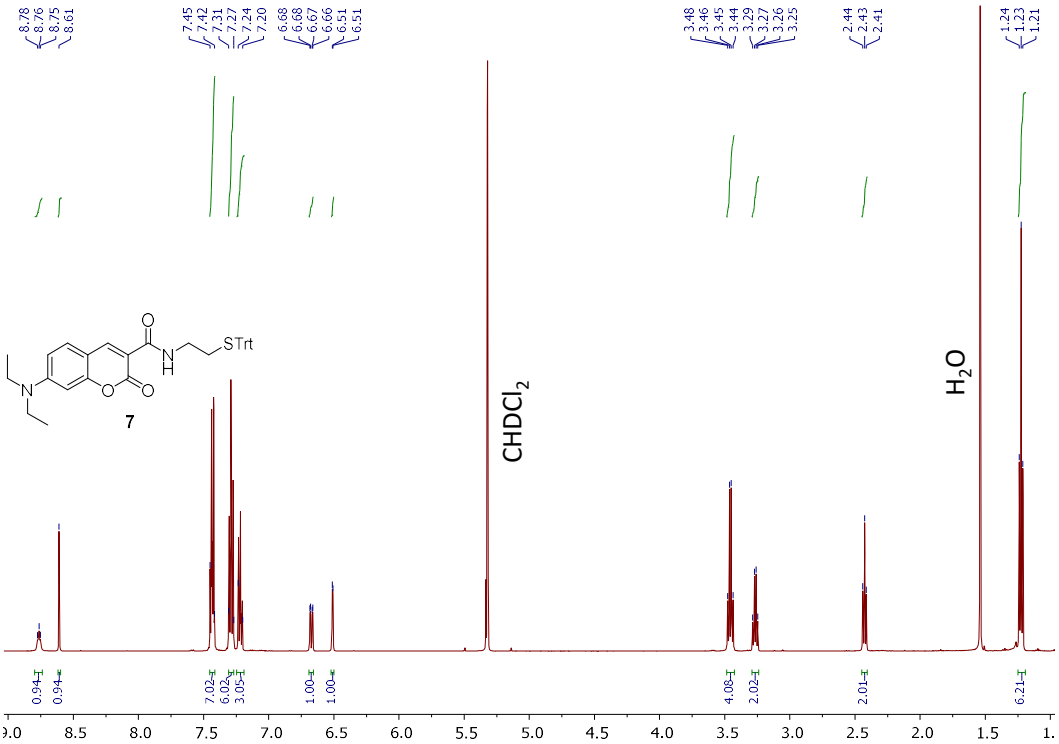

Figure S4. ^{1}H NMR of **7** in CD_2Cl_2, 500MHz, 298 K.

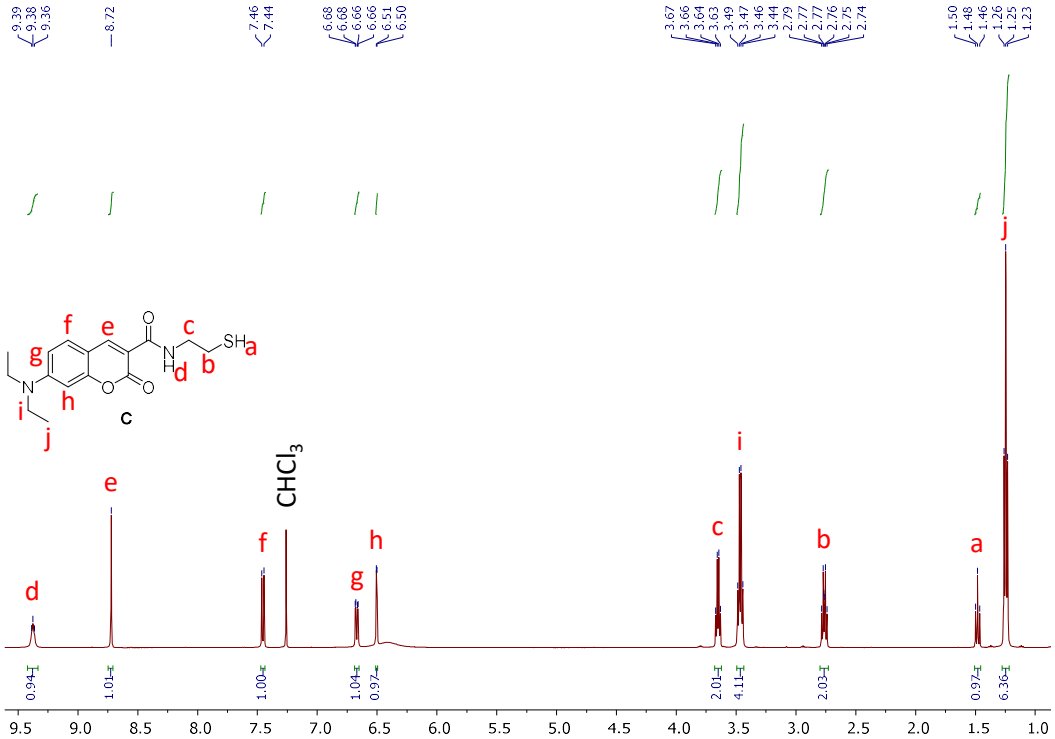

Figure S5. ^{1}H NMR of **C** in $CDCl_3$, 500 MHz, 298 K.

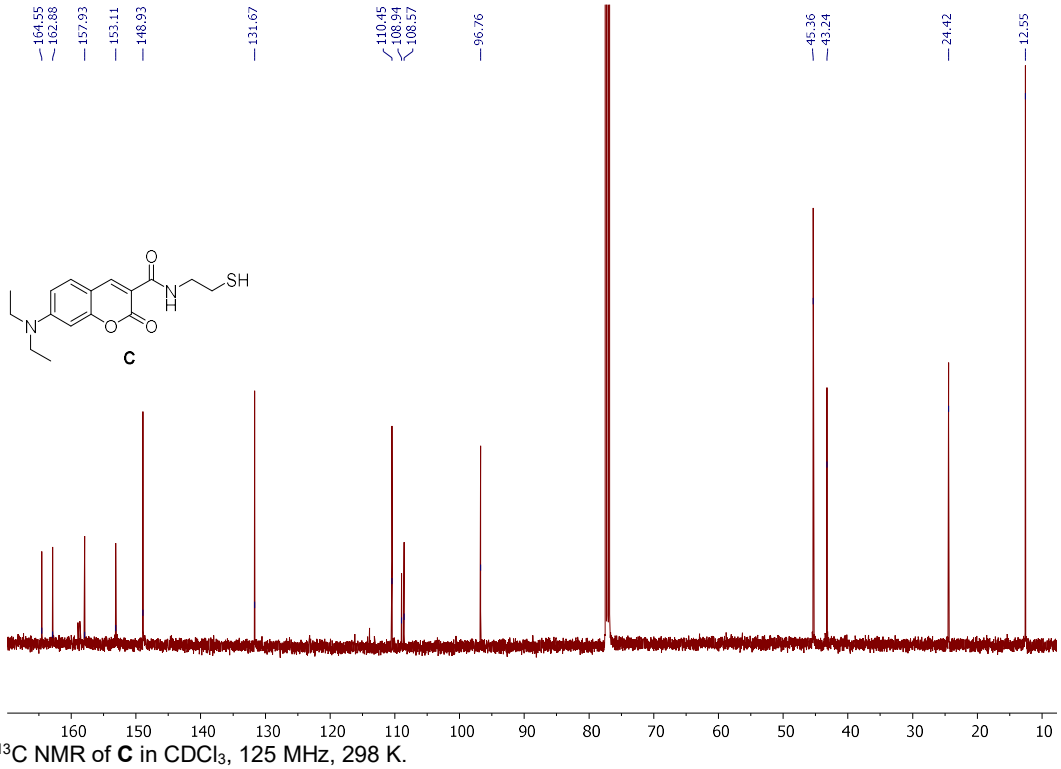

Figure S6. ^{13}C NMR of **C** in $CDCl_3$, 125 MHz, 298 K.

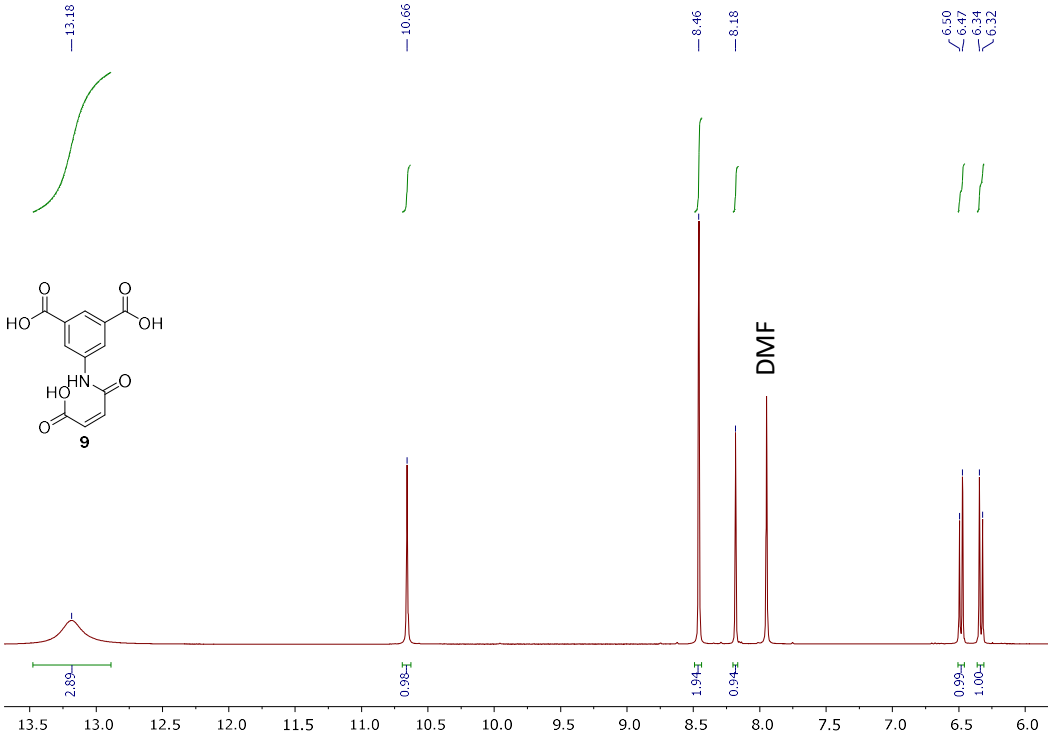

Figure S7. ^{1}H NMR of **9** in DMSO-d_6, 500 MHz, 298 K.

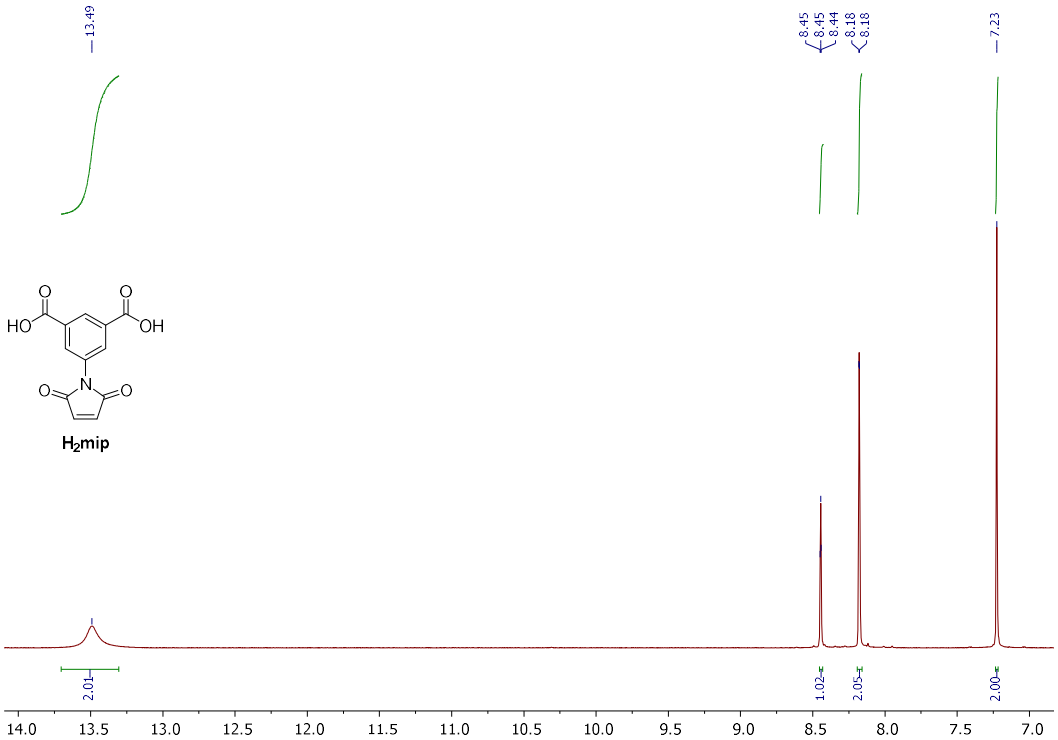

Figure S8. ^{1}H NMR of **H_2mip** in DMSO-d_6, 500 MHz, 298 K.

2. Preparation of the MCs.

2.1. Preparation of [LnGa$_4$(shi)$_4$(bz)$_4$]pym MCs.

[LnGa$_4$(shi)$_4$(bz)$_4$]pym MCs (pym = pyridinium; Ln = Y^{III}, Gd^{III}, Er^{III} and Yb^{III}; bz = benzoate) were prepared by modifying the existing procedure.[7] 306.3 mg of salicyl hydroxamic acid (2.0 mmol, 4.0 eq.) and ammonium benzoate (Y^{III}, Gd^{III}, Er^{III}: 835 mg, 6.0 mmol, 12.0 eq.; Yb^{III}: 1.11 g, 8.0 mmol, 16.0 eq.) were dissolved in 40 mL of dry methanol and 4 mL of pyridine. Ln(NO$_3$)$_3$·xH$_2$O ($5.0\cdot10^{-1}$ mmol, 1.0 eq.) and 511.4 mg of Ga(NO$_3$)$_3$ hydrate (2.0 mmol, 4.0 eq.) were dissolved in 20 mL of dry methanol each. The solution of Ga^{III} was added to the methanol/pyridine solution of salicylic hydroxamic acid and ammonium benzoate, followed by the Ln^{III} solution. The resulting solution was stirred for 1 h, filtered and set for crystallization by slow evaporation. After the solution was reduced to about one third of its initial volume, the light pink cubic crystals of [LnGa$_4$(shi)$_4$(bz)$_4$]pym were collected using a cut pipette Pasteur. In some cases, an amorphous white solid co-precipitated; its collection was carefully avoided. The complexes were washed with cold MeOH and dried in air to afford [LnGa$_4$(shi)$_4$(bz)$_4$]pym MCs as light pink cubic crystals.

[YGa$_4$(shi)$_4$(bz)$_4$]pym. The synthetic yield was 37 % based on Y(NO$_3$)$_3$·6H$_2$O. ESI-MS (MeOH/DMSO 90 : 10, soft-negative mode, m/z): [YGa$_4$(shi)$_4$(bz)$_4$]$^-$: 1452.80 (calc.), 1452.90 (exp.). Elemental analysis for [YGa$_4$(shi)$_4$(bz)$_4$]pym·1.9py: calc.: % C 50.31, % H 3.08, % N 5.74; found: % C 50.30, % H 3.04, % N 5.77.
[GdGa$_4$(shi)$_4$(bz)$_4$]pym. The synthetic yield was 42 % based on Gd(NO$_3$)$_3$·6H$_2$O. ESI-MS (MeOH/DMSO 90 : 10, soft-negative mode, m/z): [GdGa$_4$(shi)$_4$(bz)$_4$]$^-$: 1521.82 (calc.), 1521.85 (exp.). Elemental analysis for [GdGa$_4$(shi)$_4$(bz)$_4$]pym·1.7py: calc.: % C 48.10, % H 2.93, % N 5.41; found: % C 48.09, % H 2.85, % N 5.50.
[ErGa$_4$(shi)$_4$(bz)$_4$]pym. The synthetic yield was 39 % based on Er(NO$_3$)$_3$·5H$_2$O. ESI-MS (MeOH/DMSO 90 : 10, soft-negative mode, m/z): [ErGa$_4$(shi)$_4$(bz)$_4$]$^-$: 1529.82 (calc.), 1529.87 (exp.). Elemental analysis for [ErGa$_4$(shi)$_4$(bz)$_4$]pym·2.0py: calc.: % C 48.20, % H 2.96, % N 5.54; found: % C 48.18, % H 2.92, % N 5.58.
[YbGa$_4$(shi)$_4$(bz)$_4$]pym. The synthetic yield was 41 % based on Yb(NO$_3$)$_3$·5H$_2$O. ESI-MS (MeOH/DMSO 90 : 10, soft-negative mode, m/z): [YbGa$_4$(shi)$_4$(bz)$_4$]$^-$: 1535.83 (calc.), 1535.88 (exp.). Elemental analysis for [YbGa$_4$(shi)$_4$(bz)$_4$]pym·0.1H$_2$O·2.2py: calc.: % C 48.24, % H 2.99, % N 5.63; found: % C 48.26, % H 2.91, % N 5.54.

2.2. Preparation of [Ln$_2$Ga$_8$(shi)$_8$(C-mip)$_4$](HNEt$_3$)$_2$ MCs.

Despite the reaction being carried out under inert atmosphere in degassed DMF, partial thiol oxidation occurs and trace amounts of the corresponding disulfide **C$_2$** were detected by ESI-MS. They were removed by washings with DCM and MeOH. Commonly used thiol reducing agents such as dithiothreitol (DTT) or tris-(2-carboxethyl)-phosphine (TCEP) could not be used as they compete with thiols in their reaction with maleimido groups.[8,9]

2.3. ^{1}H NMR of [YGa$_4$(shi)$_4$(bz)$_4$]pym

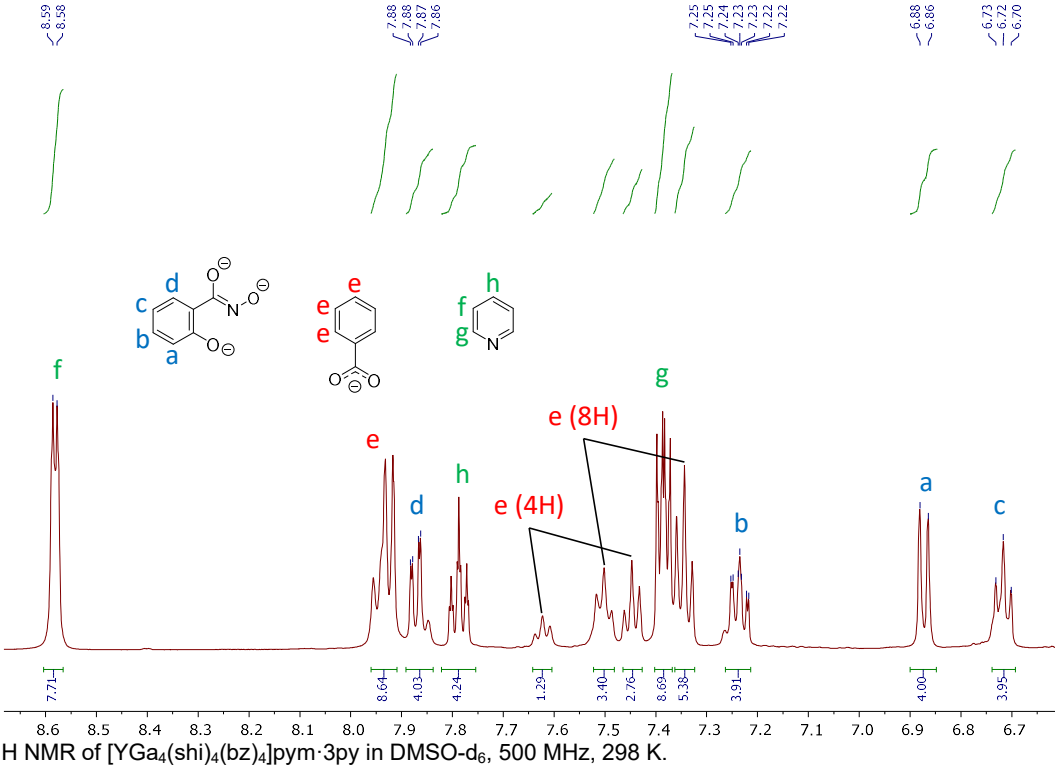

Figure S9. ^{1}H NMR of [YGa$_4$(shi)$_4$(bz)$_4$]pym·3py in DMSO-d$_6$, 500 MHz, 298 K.

2.4. ^{1}H NMR of $[Y_2Ga_8(shi)_8(mip)_4]pym_2$

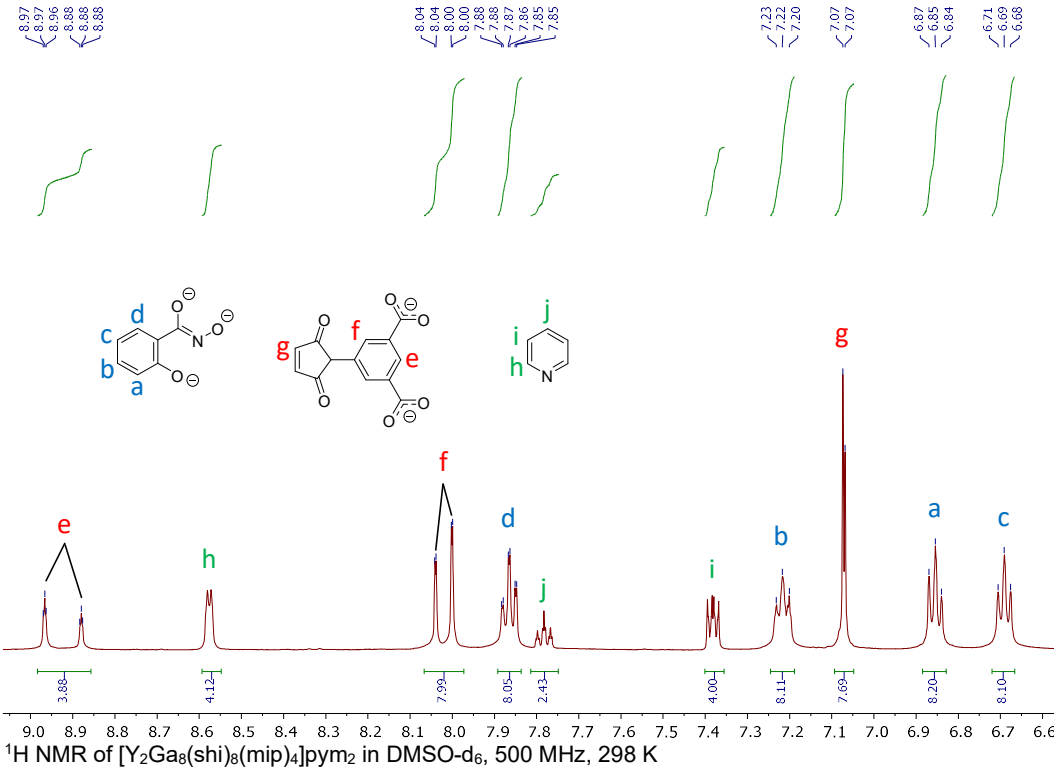

Figure S10. ^{1}H NMR of $[Y_2Ga_8(shi)_8(mip)_4]pym_2$ in DMSO-d_6, 500 MHz, 298 K

2.5. ^{1}H NMR of $[Y_2Ga_8(shi)_8(C\text{-}mip)_4](HNEt_3)_2$

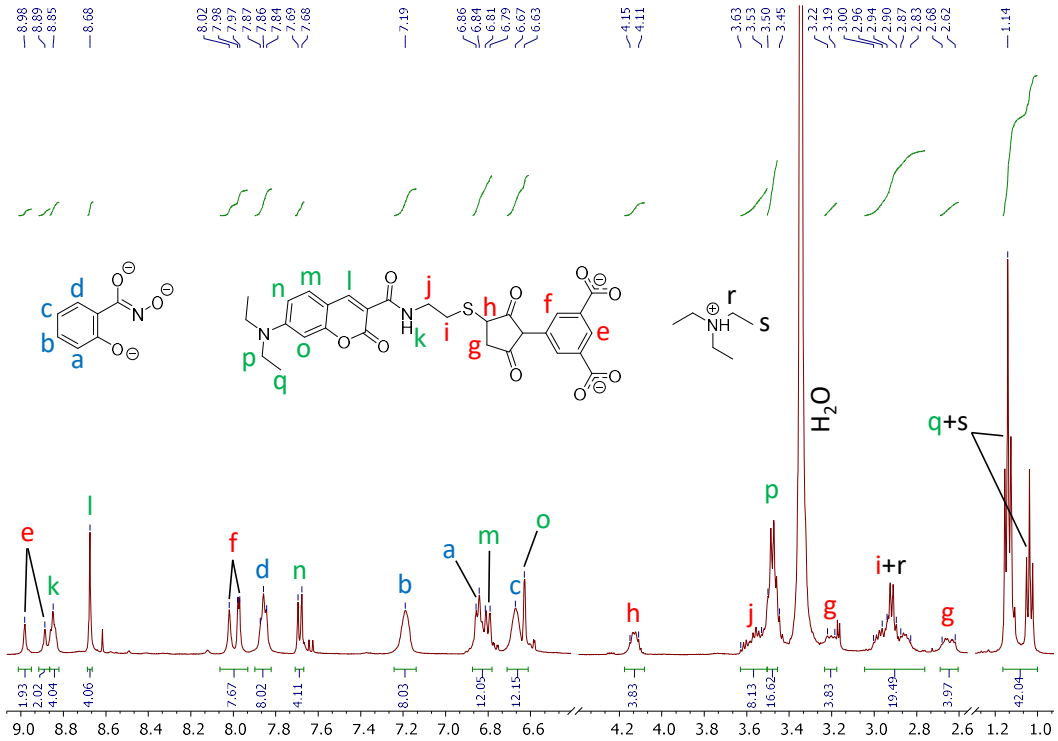

Figure S11. ^{1}H NMR of $[Y_2Ga_8(shi)_8(C\text{-}mip)_4](HNEt_3)_2$ in DMSO-d_6, 500 MHz, 298 K.

2.6. ESI-MS of MCs

The $[Ln_2Ga_8(shi)_8(C\text{-}mip)_4]^{2-}$ MCs are typically detected as $^{2-}$ adducts in negative mode ESI-MS but can also be detected as $^{2+}$ adducts in positive mode. The negative mode was used for recording purposes as degradation of the MCs occurs in the positive mode due to added formic acid in the eluent or residual traces of it when pure MeOH was used. As the molecular weights of the MCs increase, their ionization becomes less efficient, and the concentrations used were increased accordingly. Solutions of 80 and 200 μg·mL^{-1} in MeOH/DMSO 90:10 were used for $[Ln_2Ga_8(shi)_8(mip)_4]pym_2$ and $[Ln_2Ga_8(shi)_8(C\text{-}mip)_4](HNEt_3)_2$ MCs, respectively. MeOH was used as the eluent.

2.7. ESI-MS of $[Ln_2Ga_8(shi)_8(mip)_4]^{2-}$ MCs

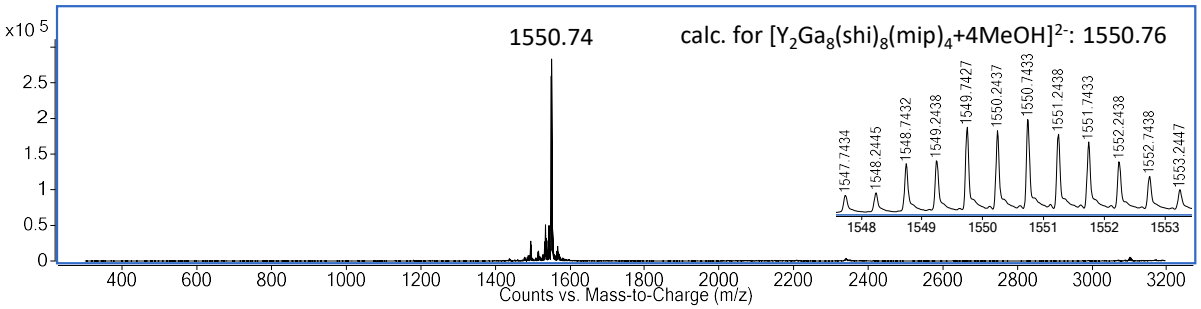

Figure S12. ESI-MS of $[Y_2Ga_8(shi)_8(mip)_4]^{2-}$ in negative mode, C_{MC} = 80 μg·mL^{-1} in MeOH/DMSO 90:10.

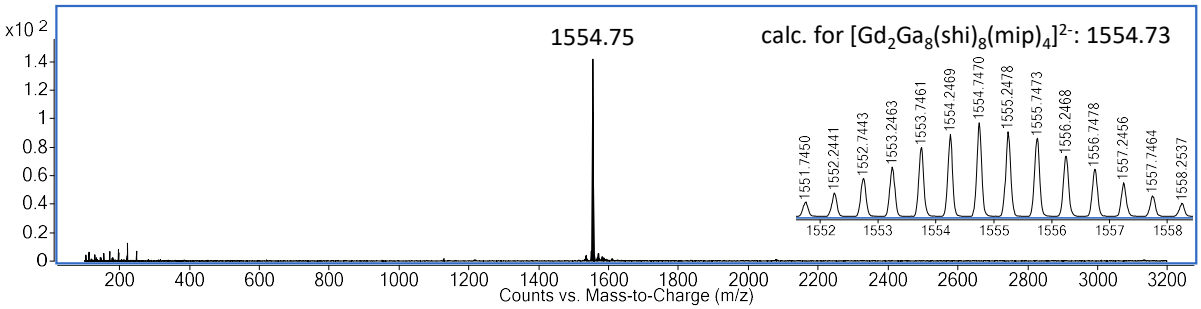

Figure S13. ESI-MS of $[Gd_2Ga_8(shi)_8(mip)_4]^{2-}$ in negative mode, C_{MC} = 80 μg·mL^{-1} in MeOH/DMSO 90:10.

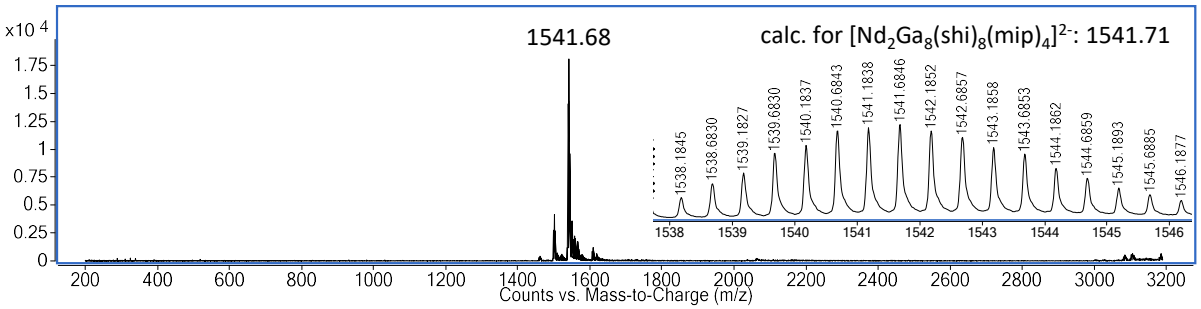

Figure S14. ESI-MS of $[Nd_2Ga_8(shi)_8(mip)_4]^{2-}$ in negative mode, C_{MC} = 80 μg·mL^{-1} in MeOH/DMSO 90:10.

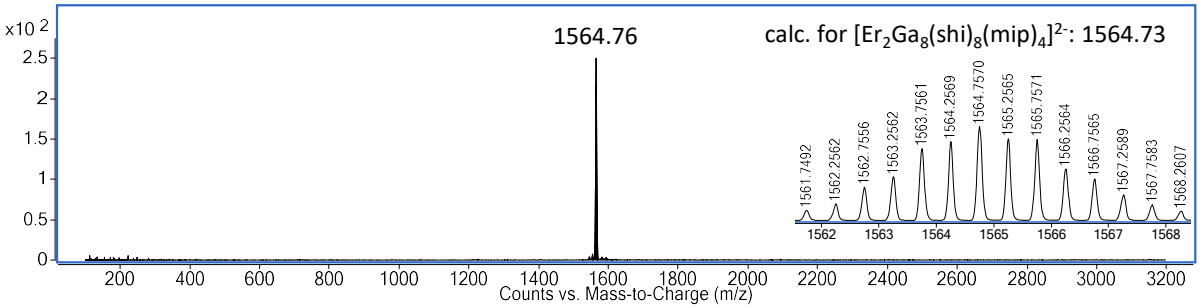

Figure S15. ESI-MS of $[Er_2Ga_8(shi)_8(mip)_4]^{2-}$ in negative mode, C_{MC} = 80 μg·mL^{-1} in MeOH/DMSO 90:10.

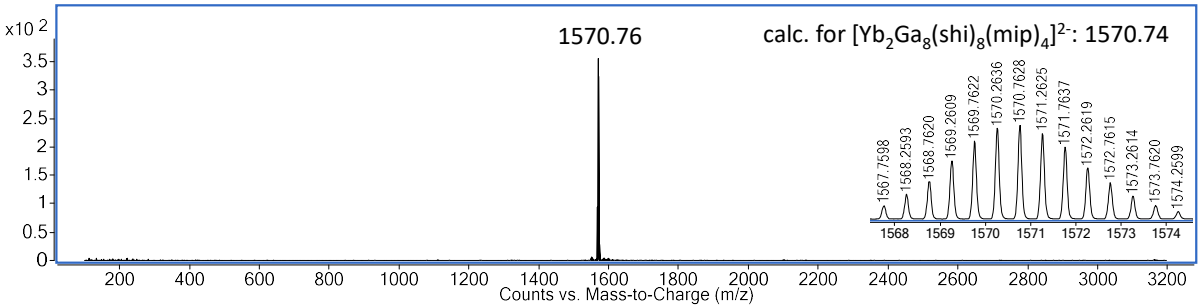

Figure S16. ESI-MS of $[Yb_2Ga_8(shi)_8(mip)_4]^{2-}$ in negative mode, C_{MC} = 80 µg·mL^{-1} in MeOH/DMSO 90:10.

2.8. ESI-MS of $[Ln_2Ga_8(shi)_8(C\text{-}mip)_4]^{2-}$ MCs

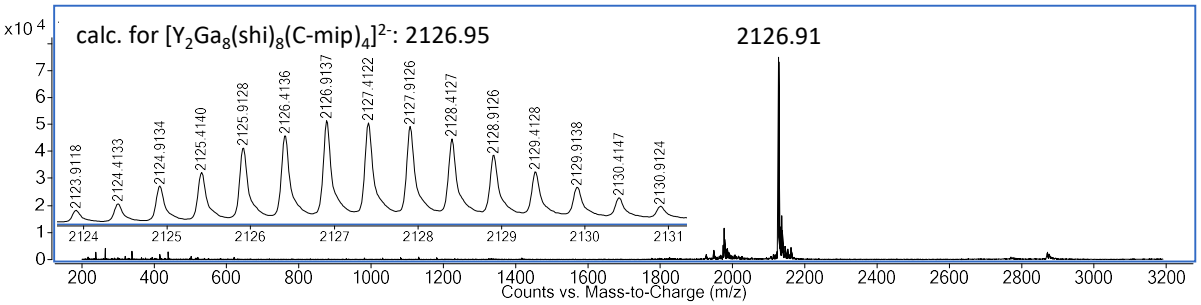

Figure S17. ESI-MS of $[Y_2Ga_8(shi)_8(C\text{-}mip)_4]^{2-}$ in negative mode, C_{MC} = 200 µg·mL^{-1} in MeOH/DMSO 90:10.

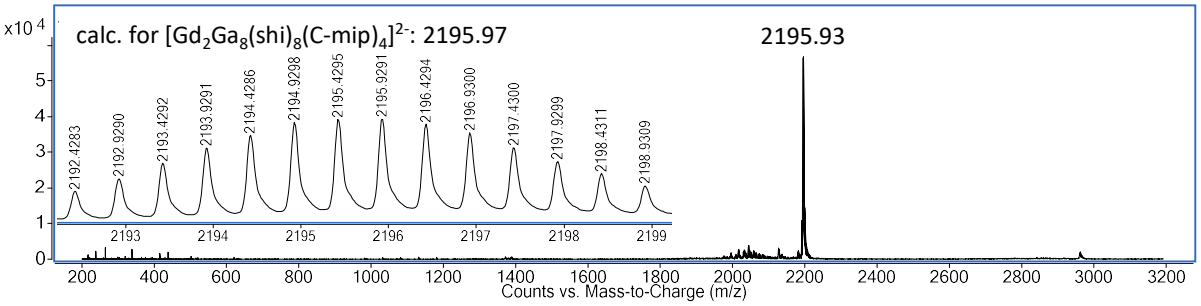

Figure S18. ESI-MS of $[Gd_2Ga_8(shi)_8(C\text{-}mip)_4]^{2-}$ in negative mode, C_{MC} = 200 µg·mL^{-1} in MeOH/DMSO 90:10.

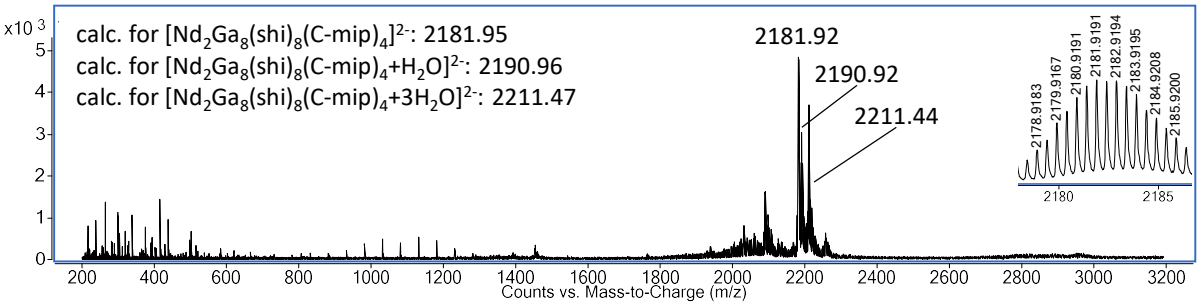

Figure S19. ESI-MS of $[Nd_2Ga_8(shi)_8(C\text{-}mip)_4]^{2-}$ in negative mode, C_{MC} = 200 µg·mL^{-1} in MeOH/DMSO 90:10.

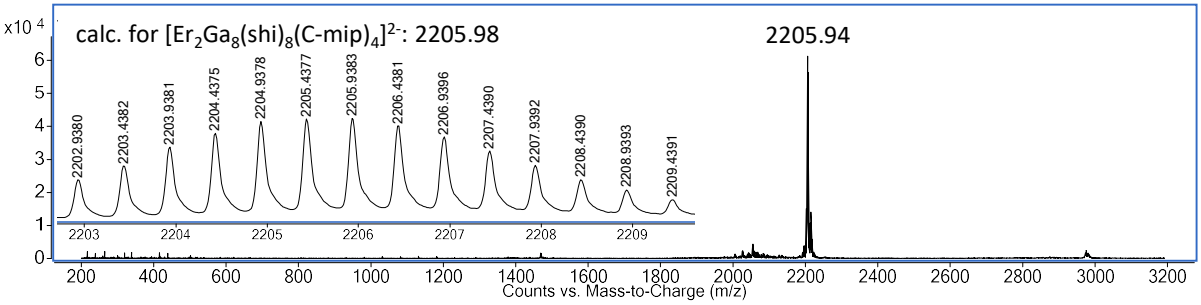

Figure S20. ESI-MS of $[Er_2Ga_8(shi)_8(C\text{-}mip)_4]^{2-}$ in negative mode, C_{MC} = 200 µg·mL^{-1} in MeOH/DMSO 90:10.

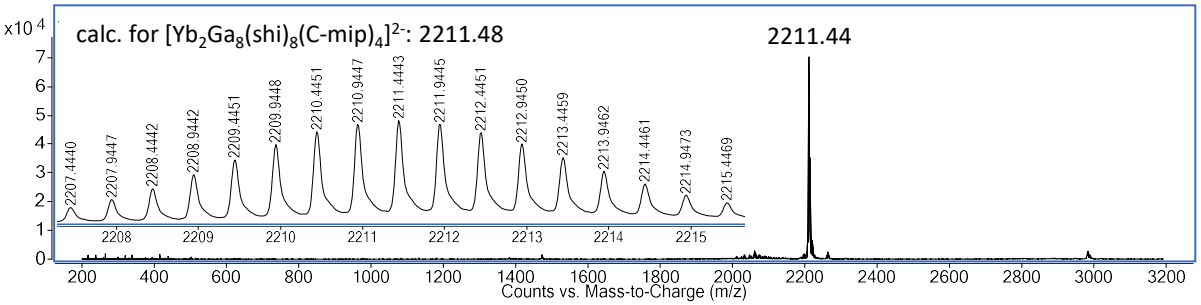

Figure S21. ESI-MS of $[Yb_2Ga_8(shi)_8(C\text{-}mip)_4]^{2-}$ in negative mode, C_{MC} = 200 μg·mL^{-1} in MeOH/DMSO 90:10.

2.9. UV-vis spectra of MCs.

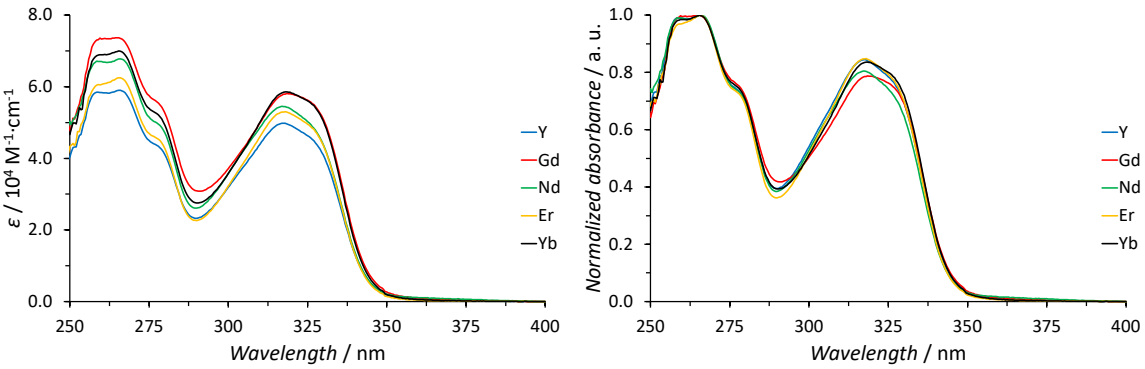

Figure S22. Molar extinction coefficients (left) and normalized UV-vis absorption (right) spectra of $[Ln_2Ga_8(shi)_8(mip)_4]^{2-}$ MCs in DMSO, 298 K.

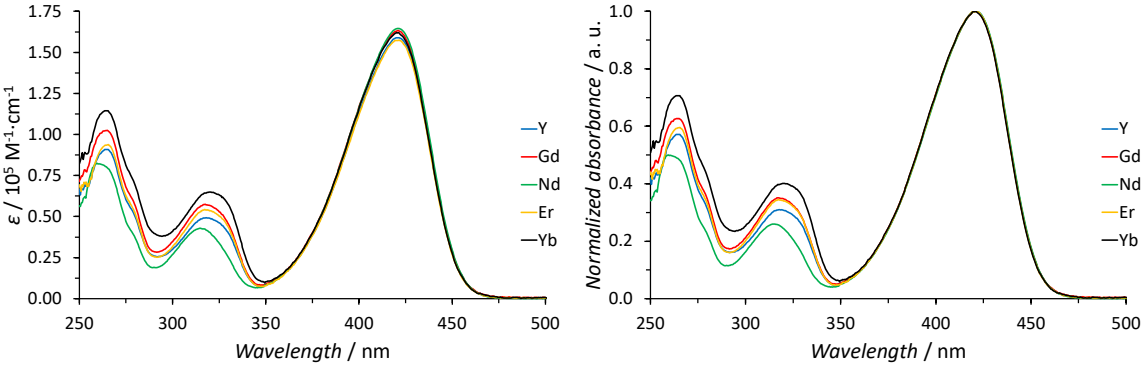

Figure S23. Molar extinction coefficients (left) and normalized UV-vis absorption (right) spectra of $[Ln_2Ga_8(shi)_8(C\text{-}mip)_4]^{2-}$ MCs in DMSO, 298 K.

2.10. ATR-FTIR spectra of MCs.

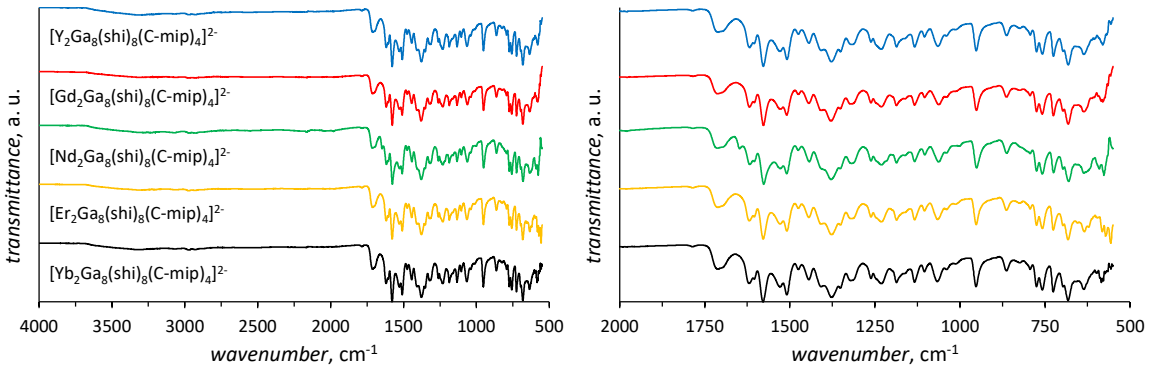

Figure S24. Solid-sate ATR-FTIR spectra of $[Ln_2Ga_8(shi)_8(C\text{-}mip)_4]^{2-}$ MCs.

3. Single crystal X-ray diffraction: structure of $[Nd_2Ga_8(shi)_8(mip)_4]^{2-}$

Single crystal X-ray crystallography. Single crystals of $[Nd_2Ga_8(shi)_8(mip)_4]^{2-}$ were coated with a trace of Fomblin oil and transferred to the goniometer head of a Bruker Quest diffractometer with a fixed chi angle, a Mo Kα wavelength (λ = 0.71073 Å) sealed fine focus X-ray tube, single crystal curved graphite incident beam monochromator and a Photon II area detector. Data were collected at 150 K (Oxford Cryosystems low temperature device), reflections were indexed and processed, and the files scaled and corrected for absorption using APEX4[10] and SADABS.[11] The space groups were assigned using XPREP within the SHELXTL suite of programs[12,13] and solved by direct methods using ShelXT[14] and refined by full matrix least squares against F^2 with all reflections using Shelxl2018[15,16] using the graphical interface Shelxle.[17] H atoms attached to carbon were positioned geometrically and constrained to ride on their parent atoms. C-H bond distances were constrained to 0.95 Å for aromatic and alkene C-H moieties, and to 0.98 Å for CH_3 moieties, respectively. Water H atom positions were refined and O-H distances were restrained to 0.84(2) Å. Where necessary, water H···H distances were restrained to 1.36(2) Å, and H atom positions were further restrained based on hydrogen bonding considerations. U_{iso}(H) values were set to a multiple of U_{eq}(C) with 1.5 for CH_3 and OH, and 1.2 for C-H units, respectively.

The deposition number CCDC 2412013 contains the supplementary crystallographic data, provided free of charge by the Cambridge Crystallographic Data Center.

The unit cell metrically fits a double orthorhombic F-centered cell but the structure realizes only monoclinic C-centered symmetry. No twinning by the higher metric symmetry was observed. Attempts have been made to refine the structure in C2 and P1 space groups (without inversion centers and mirror planes) under inclusion of possible twin operations. 1:1 disorder, however, persisted and no better fit to the data was observed. Thus, the highest possible symmetry, C2/m, was used. The four chemically equivalent hydroximate moieties (including the Ga ions and the Ga coordinated O atoms) as well as the two chemically equivalent isophthalate ligands were each restrained to have similar geometries (SAME commands of Shelx). Hydroximate benzene rings (which overlap with their counterparts created by the mirror plane) were constrained to resemble ideal hexagons with C-C distances of 1.39 Angstrom (AFIX 66 command of Shelxl). The maleimide bound to the isophthalate shows pronounced libration and rotation. No attempts were made to model disorder beyond the 1:1 systematic disorder. All maleimide bond distances and some 1,3 distances (angles) were restrained to target values (taken from CSD entry QUBQOT) as follows:

DFIX_* 1.383 N2 C16 N2 C19
DFIX_* 2.278 C16 C19
DFIX_* 1.215 C16 O9 C19 O10
DFIX_* 1.506 C16 C17 C18 C19
DFIX_* 1.319 C17 C18

Both maleimide moieties were also restrained to be close to planar. U_{ij} components of ADPs for all atoms closer to each other than 4.0 Å were restrained to be similar (SIMU 0.02 0.02 4 restraint of Shelxl). Additional disorder was observed for the "top" section of the molecules. The oxygen atom attached to one of the gallium atoms was identified as belonging to a DMF molecule. The others were refined as water molecules. Hydrogen atoms bound to these are disordered (by symmetry) with partially occupied solvate DMF molecules. All DMF molecules were restrained to have similar geometries (SAME command of Shelxl), and all DMF molecules with an occupancy smaller than 0.5 were also restrained to be close to planar. Additional electron density maxima not fitting DMF molecules were refined as partially occupied water molecules. For most sites, no attempts were made to constrain site occupancy to unity, resulting in not fully occupied sites due to unresolved (semi-liquid or highly disordered) solvate molecules. Water H atom positions were initially refined and O-H and H···H distances were restrained to 0.84(2) and 1.36(2) Å, respectively, while a damping factor was applied. H atom positions were further restrained based on hydrogen bonding considerations. In the final refinement cycles the H atoms were set to ride on their carrier oxygen atom (AFIX 3) and the damping factor was removed. Subject to these conditions, occupancies for DMF and water molecules refined to the values given in the tables of the cif. Attempts were made to localize counter-cations required for charge balance. Possible are triethyl ammonium or sodium. Within the resolved sections of the structure none could be found, making highly disordered triethyl ammonium cations residing within the unresolved solvate sections of the structure the most likely case. The structure contains additional 2582 $Å^3$ of solvent accessible voids. No substantial electron density peaks were found in the solvent accessible voids (less than 1.4 electrons per cubic Å) and the residual electron density peaks are not arranged in an interpretable pattern. The structure factors were instead augmented via reverse Fourier transform methods using the SQUEEZE routine (P. van der Sluis & A.L. Spek (1990). Acta Cryst. A 46, 194-201) as implemented in the program Platon. The resultant FAB file containing the structure factor contributions from the electron content of the void space was used in together with the original hkl file in the further refinement. (The FAB file with details of the Squeeze results is appended to the deposited cif file). The Squeeze procedure corrected for 512 electrons within the solvent accessible voids.

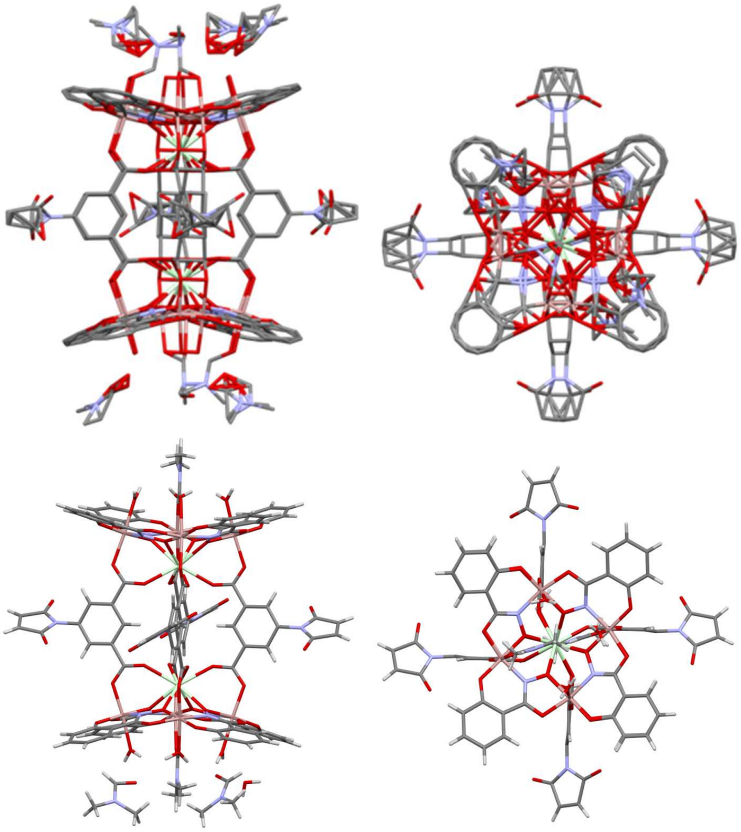

Figure S25. Structure of $[Nd_2Ga_8(shi)_8(mip)_4]^{2-}$ obtained from X-ray diffraction on single crystals (deposition number CCDC 2412013). Color code: Nd^{III}: cyan; Ga^{III}: rose; O: red; N: light blue; C: grey. Top row: Most disordered moieties shown. Left: side view; right: top-down view. Hydrogen atoms are omitted for clarity. Solvent molecules: three water and one molecule of DMF are coordinated to the Ga^{III} atoms. More disordered DMF molecules form hydrogen bonds to these three water molecules. Bottom row: symmetry created atoms and less than half occupied moieties omitted. Left: side view; right: top-down view. Solvate molecules only shown for bottom half of side view.

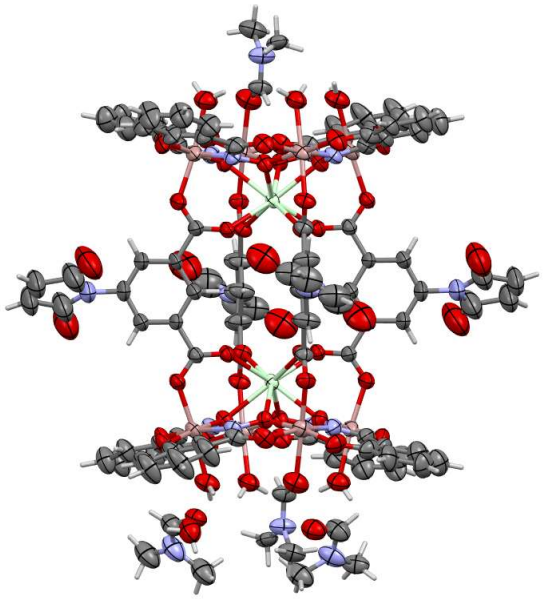

Figure S26. Ellipsoid plot at the 50% probability level of the $[Nd_2Ga_8(shi)_8(mip)_4]^{2-}$ MC (deposition number CCDC 2412013). Symmetry created atoms and less than half occupied moieties omitted. Solvate molecules only shown for bottom half.

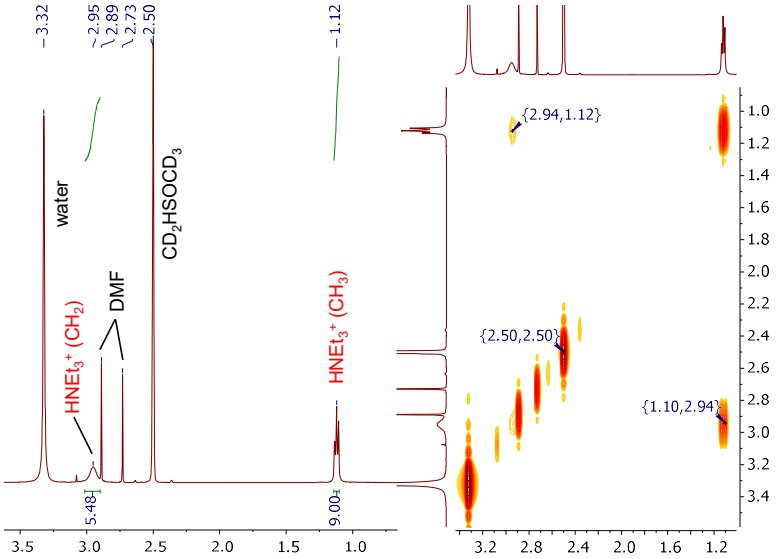

Figure S27. Confirmation of $HNEt_3^+$ acting as a counter-cation in the isolated $[Nd_2Ga_8(shi)_8(mip)_4](HNEt_3)_2$ MC. ^1H NMR (left) and COSY (right) in DMSO-d_6, 500 MHz, 298 K. As expected, the CH_3-CH_2 correlation in $HNEt_3^+$ can be seen on the right. The peaks are shifted compared to what is expected for free NEt_3: $\delta(CH_3)_{exp}$ = 1.12 ppm; $\delta(CH_3)_{reported}$ = 0.93 ppm (DMSO-d_6)[18] and $\delta(CH_2)_{exp}$ = 2.95 ppm; $\delta(CH_2)_{reported}$ = 2.43 ppm (DMSO-d_6).[18] This is likely due to the protonation in the $HNEt_3^+$ counter-cation and its proximity with the paramagnetic Nd^{III} MC, further evidenced by the loss of the hyperfine structure of CH_2 in $HNEt_3^+$ (bs instead of q).

Table S1. Crystallographic data for $[Nd_2Ga_8(shi)_8(mip)_4]^{2-}$

Compound	$[Nd_2Ga_8(shi)_8(mip)_4]^{2-}$
Chemical formula	$C_{107}H_{71}Ga_8Nd_2O_{56}\cdot 3.22DMF\cdot 1.87H_2O$
Formula weight	3549.90 g/mol
Crystal system, space group, Hall group	monoclinic, C 2/m, -C 2y
T	150 K
A	25.4801(15) Å
B	23.6113(15) Å
C	20.8659(15) Å
A	90°
β	127.581(4)°
γ	90°
Volume	9948.4(12) $Å^3$
λ	0.71073 Å
ρ_{calc}	1.185 g/cm^3
Z	2
Absorption coefficient	1.647 mm^{-1}
F(000)	3535.0
θ range for data collection	2.017 to 30.562°
Limiting indices	-26 ≤ h ≤ 36
	-32 ≤ k ≤ 33
	-29 ≤ l ≤ 29
Reflection collected / unique	52127 / 15485
Completeness to θ	99.3%
Absorption correction	multi-scan
Refinement method	Full-matrix least-squares on F^2
data / restraints / parameters	15485 / 4610 /1017
Goodness of fit on F^2	1.032
R_1(reflections) [a]	0.0636(12656)
wR_2(reflections) [b]	0.1958(15485)
Largest diff. peak and hole	1.358, -1.544

[a] $R_1 = \Sigma(||F_o|-|F_c||)/\Sigma|F_o|$ [b] $wR_2 = [\Sigma[w(F_o^2 - F_c^2)^2]/\Sigma[w(F_o)^2]]^{1/2}$; $w = 1/[\sigma^2(F_o^2) + (0.1210p)^2 + 21.0918p]$; $p = [\max(F_o^2,0) + 2F_c^2]/3$ (*m* and *n* are constants); $\sigma = [\Sigma[w(F_o^2 - F_c^2)^2/(n-p)]^{1/2}$

Table S2. SHAPE[19,20] analysis of various [$LnGa_4$] and [Ln_2Ga_8] MCs.

MC	$[DyGa_4(shi)_4(bz)_4]^-$	$[Dy_2Ga_8(shi)_8(ip)_4]^{2-}$	$[Sm_2Ga_8(eshi)_8(ip)_4]^{2-}$	$[Nd_2Ga_8(shi)_8(mip)_4]^{2-}$
Reference	[7]	[21]	[1]	this work
OP [a]	29.684	29.638	29.964	29.878
HPY [a]	23.667	23.294	23.594	23.603
HPBY [a]	16.364	16.136	16.574	16.952
CU [a]	9.108	8.718	9.314	9.385
SAPR [a]	**0.394**	**0.419**	**0.630**	**0.501**
TDD [a]	2.332	2.389	2.680	2.659
JGBF [a]	16.469	16.354	16.724	17.198
JETBPY [a]	29.309	29.175	29.194	29.523
JBTP [a]	2.893	2.805	2.807	2.925
BTPR [a]	1.855	1.817	1.531	1.710
JSD [a]	5.444	5.479	5.775	5.724
TT [a]	9.940	9.559	10.156	10.243
ETBPY [a]	24.364	24.322	24.322	24.881

[a] OP: octagon, D_{8h}; HPY: heptagonal pyramid, C_{7v}; HBPY: hexagonal bipyramid, D_{6h}; CU: Cube, O_h; SAPR: square antiprism, D_{4d}; TDD: triangular dodecahedron, D_{2d}; JGBF: Johnson – gyrobifastigium (J26), D_{2d}; JETBPY: Johnson – elongated triangular bipyramid (J14), D_{3h}; JBTP: Johnson – biaugmented trigonal prism (J50), C_{2v}; BTPR: biaugmented trigonal prism, C_{2v}; JSD: snub disphenoid (J84), D_{2d}; triakis tetrahedron, T_d; ETBPY: elongated trigonal bipyramid, D_{3h}.

4. Photophysical properties of MCs

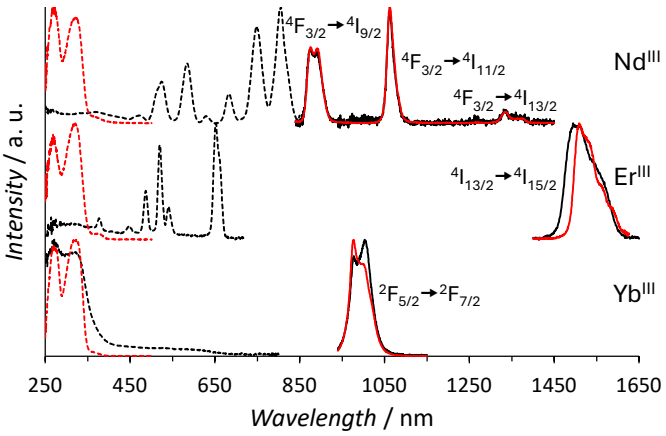

Figure S28. Corrected and normalized emission (full lines) and excitation (dotted lines) spectra for $[Ln_2Ga_8(shi)_8(mip)_4]^{2-}$ MCs at 298 K, 50 μM in DMSO (red lines) and in the solid state (black lines). Emission: λ_{exc} = 320 nm (DMSO) and 340 nm (solid state). Excitation: λ_{em} = 1063 nm, 1524 nm and 991 nm for Nd^{III}, Er^{III} and Yb^{III} analogues, respectively.

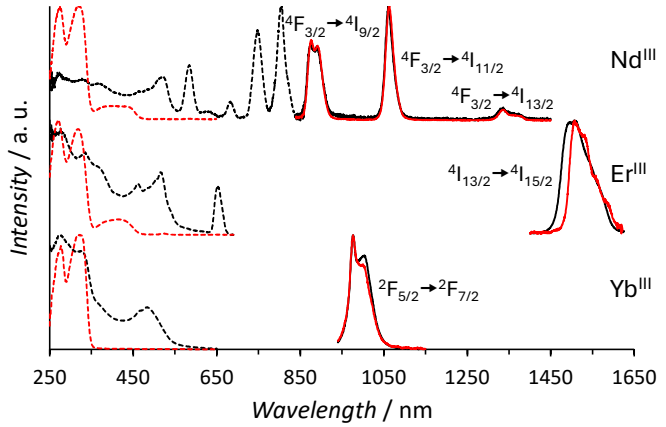

Figure S29. Corrected and normalized emission (full lines) and excitation (dotted lines) spectra for $[Ln_2Ga_8(shi)_8(C\text{-}mip)_4]^{2-}$ MCs at 298 K, 50 μM in DMSO (red lines) and in the solid state (black lines). Emission: λ_{exc} = 420 nm (DMSO) and 465 nm (solid state). Excitation: λ_{em} = 1063 nm, 1524 nm and 991 nm for Nd^{III}, Er^{III} and Yb^{III} analogues, respectively.

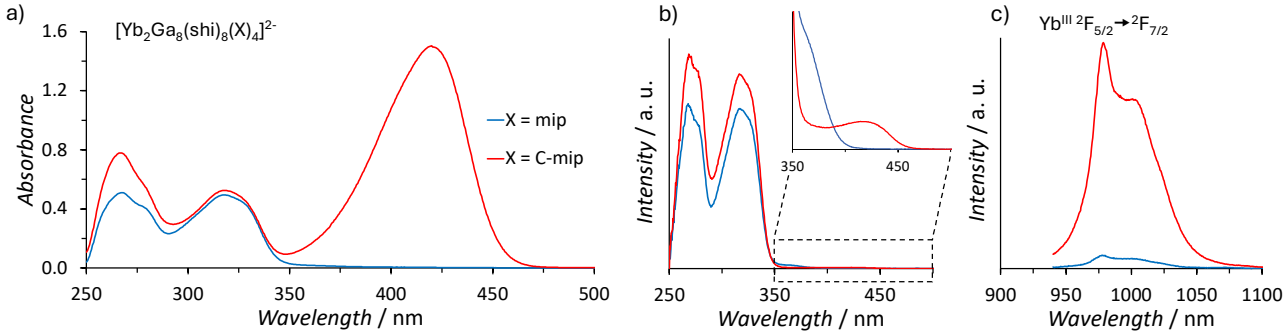

Figure S30. Comparison of the photophysical properties of the $[Yb_2Ga_8(shi)_8(mip)_4]^{2-}$ (in blue) and $[Yb_2Ga_8(shi)_8(C\text{-}mip)_4]^{2-}$ (in red) MCs in DMSO at 298 K. Suprasil® quartz cuvettes of l = 2 mm were used and spectra were recorded using the same experimental parameters for both MCs. a) UV-vis absorption spectra, C_{MC} = 50 μM. b) Excitation spectra (λ_{em} = 991 nm), C_{MC} = 10 μM. Inset: excitation spectra in the 350–500 nm range (λ_{em} = 991 nm), C_{MC} = 10 μM. c) Emission spectra depicting the intensity of the emission band of the Yb^{III} $^2F_{5/2}\rightarrow{}^2F_{7/2}$ electronic transition at λ_{em} = 991 nm upon excitation at λ_{exc} = 420 nm, C_{MC} = 50 μM.

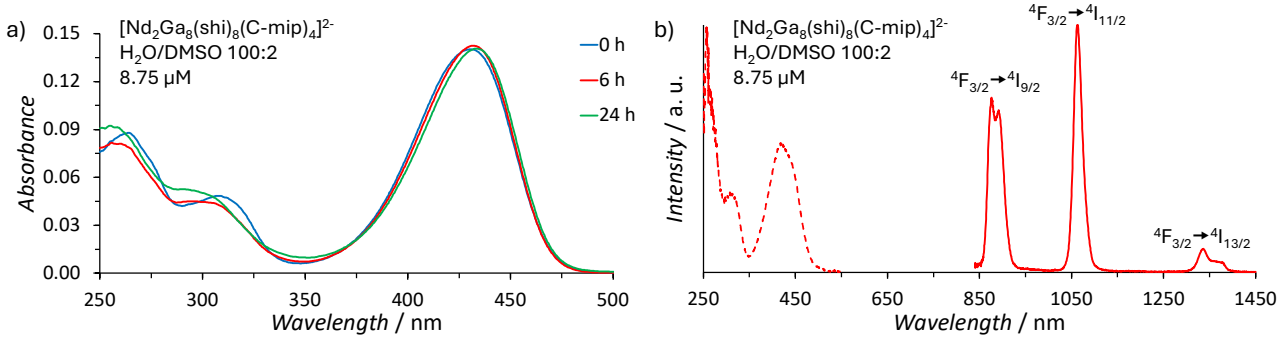

Figure S31. Photophysical properties of the $[Nd_2Ga_8(shi)_8(C\text{-}mip)_4]^{2-}$ MC in aqueous media (H_2O/DMSO 100:2) at the concentration used for cell imaging experiments (C_{MC} = 8.75 μM). a) UV-vis absorption spectra. b) Excitation (dotted line, λ_{em} = 1063 nm) and emission spectra (λ_{exc} = 420 nm).

Table S3. Ln^{III}-centered quantum yields (Q_{Ln}^L) and observed luminescence lifetimes (τ_{obs}) of $[Ln_2Ga_8(shi)_8(C\text{-}mip)_4]^{2-}$ MCs in solution and in the solid state (SS) at 298 K.

MC	Conditions	λ_{exc} nm	Q_{Ln}^L %	τ_{obs}[a] μs
$[Nd_2Ga_8(shi)_8(C\text{-}mip)_4]^{2-}$	DMSO, 50 μM	420	$4.5(1)\cdot10^{-2}$	2.44(4)
	H_2O/DMSO 100:2, 8.75 μM	420	$3.4(2)\cdot10^{-2}$	0.58(1)
	SS	465	$5.1(3)\cdot10^{-2}$	0.82(3)
$[Er_2Ga_8(shi)_8(C\text{-}mip)_4]^{2-}$	DMSO, 50 μM	420	$4.8(3)\cdot10^{-3}$	7.63(5)
	SS	465	$5.3(2)\cdot10^{-3}$	3.7(1)
$[Yb_2Ga_8(shi)_8(C\text{-}mip)_4]^{2-}$	DMSO, 50 μM	420	$2.12(3)\cdot10^{-2}$	53.2(6)
	SS	465	0.28(3)	23.6(2)

[a] λ_{exc} = 355 nm.

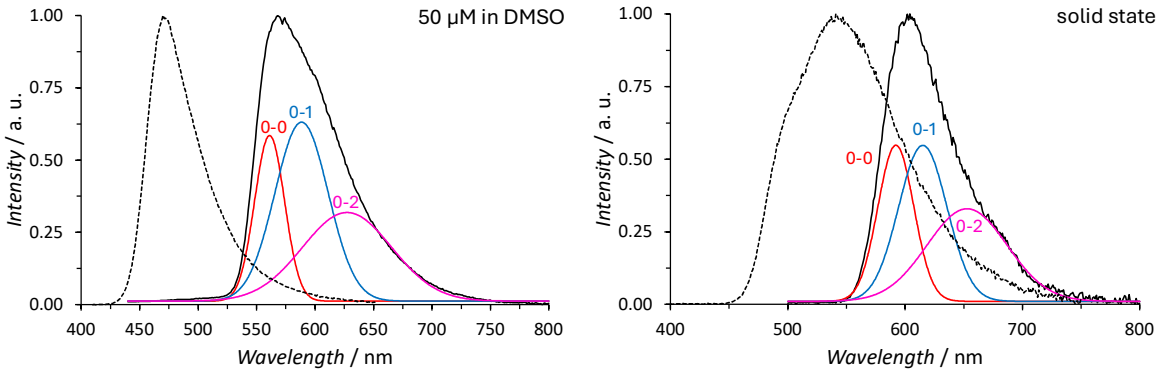

Figure S32. Recorded fluorescence (black dotted line) and phosphorescence (black full line) spectra of the $[Gd_2Ga(shi)_8(C\text{-}mip)_4]^{2-}$ MC. Left: 50 µM DMSO solution, 298 K (fluo.) and 77 K (phos.), λ_{exc} = 420 nm, T_1 = 17825 cm^{-1} (0-0 Gaussian). Right: solid state, 298 K (fluo.) and 77 K (phos.), λ_{exc} = 420 nm, τ_{delay} = 500 µs; T_1= 16890 cm^{-1} (0-0 Gaussian). Colored lines: Gaussian deconvolution of the recorded phosphorescence spectra. The deconvolution of the experimental phosphorescence spectra was performed by fitting the experimental data with the Origin software[22] using three Gaussian curves.

5. NIR imaging of living HeLa cells

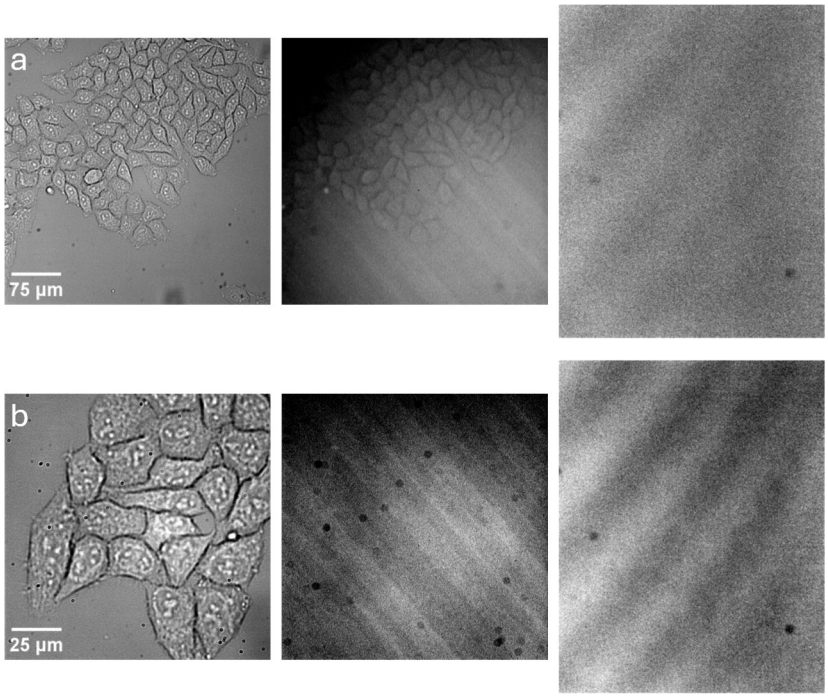

Figure S33. Control images obtained from epifluorescence microscopy experiments on living HeLa cells incubated for 3 h with 2% DMSO in Opti-MEM. From left to right: brightfield image (exposition time: 10 ms), visible emission (λ_{exc}: BP414/46 nm; λ_{em}: BP482/35 nm; exposition time: 10 ms), NIR emission (λ_{exc}: BP417/60 nm; λ_{em}: BP1065/30 nm; exposition time: 5 s). (a) 20× magnification objective. (b) 60× magnification objective. Images within the same row share the same scale bar.

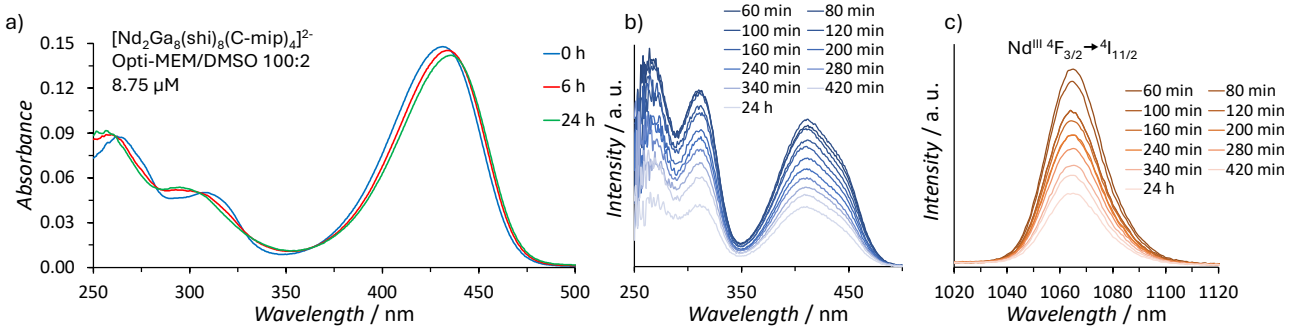

Figure S34. Stability of the $[Nd_2Ga_8(shi)_8(C\text{-}mip)_4]^{2-}$ MC over time under the conditions used for NIR imaging of living HeLa cells (Opti-MEM/DMSO 100:2; C_{MC} = 8.75 µM, 298 K). a) UV-vis absorption spectra. b) Excitation spectra (λ_{em} = 1063 nm). c) Emission spectra depicting the Nd^{III} $^4F_{3/2}\rightarrow{}^4I_{11/2}$ electronic transition at λ_{em} = 1063 nm (λ_{exc} = 420 nm).

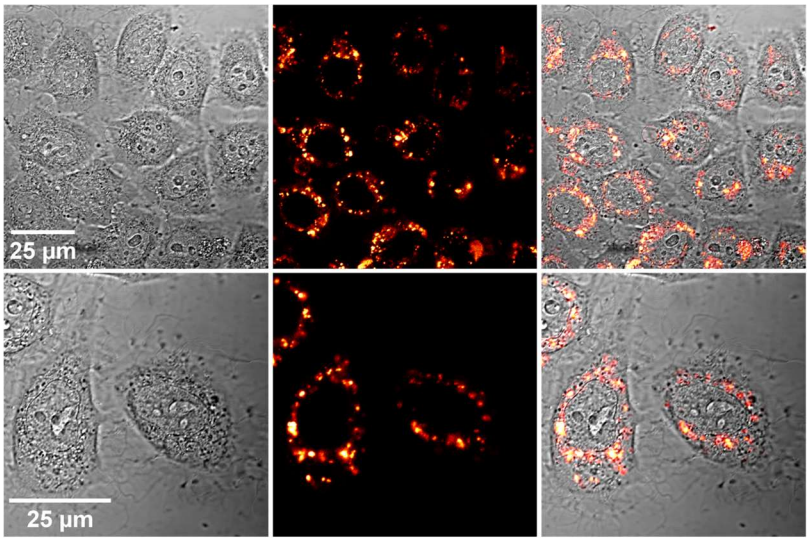

Figure S35. Images obtained from confocal microscopy experiments on HeLa cells incubated with the $[Nd_2Ga_8(shi)_8(C\text{-}mip)_4]^{2-}$ MC at 40 µg·mL^{-1} for 3 h. From left to right: brightfield image, visible fluorescence (λ_{exc}: 405 nm; λ_{em}: 475–600 nm) and merged images. 60× magnification objective. Images within the same row share the same scale bar.

6. References

1 J. C. Lutter, B. A. Lopez Bermudez, T. N. Nguyen, J. W. Kampf and V. L. Pecoraro, *J. Inorg. Biochem.*, 2019, **192**, 119–125.
2 H. G. Ghalehshahi, S. Balalaie and A. Aliahmadi, *New J. Chem.*, 2018, **42**, 8831–8842.
3 R. Maggi, F. Bigi, S. Carloni, A. Mazzacani and G. Sartori, *Green Chem.*, 2001, **3**, 173–174.
4 T. P. Gustafson, G. A. Metzel and A. G. Kutateladze, *Org. Biomol. Chem.*, 2011, **9**, 4752–4755.
5 S. Fiorito, V. A. Taddeo, S. Genovese and F. Epifano, *Tetrahedron Lett.*, 2016, **57**, 4795–4798.
6 A. A. Watrelot, D. T. Tran, T. Buffeteau, D. Deffieux, C. Le Bourvellec, S. Quideau and C. M. G. C. Renard, *Appl. Surf. Sci.*, 2016, **371**, 512–518.
7 C. Y. Chow, S. V. Eliseeva, E. R. Trivedi, T. N. Nguyen, J. W. Kampf, S. Petoud and V. L. Pecoraro, *J. Am. Chem. Soc.*, 2016, **138**, 5100–5109.
8 S. N. Mthembu, A. Sharma, F. Albericio and B. G. de la Torre, *ChemBioChem*, 2020, **21**, 1947–1954.
9 S. D. Fontaine, R. Reid, L. Robinson, G. W. Ashley and D. V. Santi, *Bioconjug. Chem.*, 2015, **26**, 145–152.
10 Apex3, v2019.1-0, SAINT V8.40A, 2019, Bruker AXS Inc., Madison (WI), USA.
11 L. Krause, R. Herbst-Irmer, G. M. Sheldrick and D. Stalke, *J. Appl. Crystallogr.*, 2015, **48**, 3–10.
12 SHELXTL suite of programs, Version 6.14, 2000-2003, Bruker Advanced X-ray Solutions, Bruker AXS Inc., Madison (WI), USA.
13 G. M. Sheldrick, *Acta Crystallogr. A*, 2008, **64**, 112–122.
14 G. M. Sheldrick, *Acta Crystallogr. Sect. Found. Adv.*, 2015, **71**, 3–8.
15 G. M. Sheldrick, *Acta Crystallogr. Sect. C Struct. Chem.*, 2015, **71**, 3–8.
16 G. M. Sheldrick, SHELXL-2019, Program for the Refinement of Crystal Structures, University of Göttingen, Germany, 2019.
17 C. B. Hübschle, G. M. Sheldrick and B. Dittrich, *J. Appl. Crystallogr.*, 2011, **44**, 1281–1284.
18 G. R. Fulmer, A. J. M. Miller, N. H. Sherden, H. E. Gottlieb, A. Nudelman, B. M. Stoltz, J. E. Bercaw and K. I. Goldberg, *Organometallics*, 2010, **29**, 2176–2179.
19 S. Alvarez, P. Alemany, D. Casanova, J. Cirera, M. Llunell and D. Avnir, *Coord. Chem. Rev.*, 2005, **249**, 1693–1708.
20 D. Casanova, M. Llunell, P. Alemany and S. Alvarez, *Chem. – Eur. J.*, 2005, **11**, 1479–1494.
21 T. N. Nguyen, C. Y. Chow, S. V. Eliseeva, E. R. Trivedi, J. W. Kampf, I. Martinić, S. Petoud and V. L. Pecoraro, *Chem. – Eur. J.*, 2018, **24**, 1031–1035.
22 Origin, 9.0.0, 1991-2012, OriginLab Corporation, Northampton (MA), USA.